JOURNAL OF MATERIALS SCIENCE 27 (1992) 2841–2847

Phase transformations in the BiSrCaCuO system for thick films from a novel nitrate paste

L. A. STROM*, G. PAZ-PUJALT, L. BOSWORTH
Corporate Research Laboratories, Eastman Kodak Company, Rochester, New York 14650, USA

This study focuses on the phase changes occurring in superconducting thick films of $Bi_2Sr_2Ca_1Cu_2O_x$ printed from a novel nitrate paste on single-crystal MgO. By optimizing the firing profile, the ratio of the 2.4 nm to 3.0 nm phase could be controlled to achieve reproducible T_0 values of 85 K. A model for the 2.4 nm to 3.0 nm phase transformation is proposed, based on SEM and X-ray diffraction data. Two unit cells of the 2.4 nm phase may transform to one 3.0 nm phase unit cell by losing two bismuth oxide layers and one strontium oxide layer. Sr, Bi-rich particles were observed by SEM after the transformation. The degradation of the thick films with ageing at room temperature may be related to possible $SrCO_3$ and/or $CaCO_3$ formation.

1. Introduction

Over the last two years, high T_c ceramic superconductors have stimulated the interest of many researchers because of their potential to have a large impact on microelectronics, medicine, and transportation. Three of the systems which have generated a great deal of excitement are LaSrCuO, TlBaCaCuO, and YBaCuO. The BiSrCuO system also has been of some interest because its new structure might give insight on the mechanism for superconductivity in oxides. The temperature at which the material achieves complete superconductivity, T_0, was only 8 K, however [1]. When Maeda *et al.* [2] added Ca to the bismuth system and discovered a potential T_0 of 105 K, more researchers began to work on this system. Since then it has been discovered that at least three superconducting phases exist in the BiSrCaCuO system. The phases are pseudotetragonal with *a*-axis dimensions of approximately 0.54 nm and variable *c*-axis dimensions of approximately 2.4, 3.0 and 3.7 nm. The T_0 values of these phases are approximately 7, 80 and 105 K, respectively [2, 3].

The 2.4 nm phase appears to be similar to the 2.46 nm phase $Bi_2Sr_2Cu_1O_x$ [4]. In this case, a solid solution of Sr and Ca gives the formula $Bi_2(SrCa)_2Cu_1O_x$. It is believed that the 3.0 nm phase can be derived from the 2.4 nm phase by the addition of a CuO_2 layer and a CaSr layer [5, 6]. The 3.0 nm phase $Bi_2(SrCa)_3Cu_2O_x$ (2212) has been characterized [7]. It is believed that vacancies in the Ca/Sr layer between the CuO_2 layers provide current paths for superconductivity [8]. Oxygen vacancies would result in a coordination number of 8, which favours Ca over Sr in this layer because of its smaller size. This may explain why the Ca addition is so beneficial to superconductivity in this system [8]. Some substitution of Ca by Bi is seen by high-resolution electron microscopy (HREM) and may play an important role in superconductivity [9]. Modulations along the *b*-axis have also been seen by HREM, thus explaining the pseudotetragonal nature seen by X-ray diffraction (XRD) [7, 10, 11]. The 3.7 nm phase $Bi_2(SrCa)_4Cu_3O_x$ (2223) with a T_c of 110 K and a T_0 of approximately 105 K can be derived from the 3.0 nm phase by the addition of a CuO_2 layer and an Sr/Ca layer [5, 6]. This phase has been difficult to synthesize, however. It is generally observed only in samples that have been processed near their melting point and fired for very long times [11, 12]. It is most often detected in samples rich in Cu (1112 = 2224). Additions of Pb have been found to be helpful in increasing the volume per cent of the 110 K phase and in achieving superconductivity above 100 K [13].

Screen-printed thick films of 1112 containing predominantly the 3.0 and 3.7 nm phases have been made on single-crystal MgO. The paste used for screen printing was made by the traditional calcined-powder-plus-polymer method. The films showed large changes in resistivity at 110 K and at least one of the samples was completely superconducting at 107 K [14, 15]. Screen-printed films of 1112 were found to have T_0 values of 76 K on Ag tape [15], 70 K on Ni tape [15], 63–65 K on yttria-stabilized zirconia (YSZ) [16], and 11 K on $SrTiO_3$ [16]. However, 1112 was found not to be superconducting on alumina and quartz [16]. The composition 2213 also was superconducting on YSZ with a T_0 of approximately 68 K [16]. Controlling the ratio of the 2.4 nm to 3.0 nm phase appeared to be critical in achieving superconductivity on $SrTiO_3$ and YSZ. The ratio was found to be dependent on both the substrate and firing temperature [16].

* *Current address*: Hi-Tech Ceramics, PO Box 788, Alfred, NY 14802, USA

Other methods which have been proposed for making thick films in the bismuth system are spray pyrolysis and melt quenching. The spray pyrolysis method, as described by Nobumasa *et al.* [17], involved spraying a solution of Bi, Pb, Sr, Ca and Cu nitrates in a 0.8:0.2:0.8:1.7:1.6 ratio on single-crystal MgO. The substrate was heated to 400 °C during deposition. Heat treatments at 845 °C for 2–80 h were necessary to obtain superconductivity in the films. Heat treatment for 15 h at 845 °C gave the largest amount of the 3.7 nm phase; this film became completely superconducting above 100 K. Film composition did not remain constant, however. Pb, Ca and Sr were lower in the fired film than in the starting solution [17]. The loss of Pb is easily explainable due to the known vaporization of Pb above 800 °C. Ca and Sr may be lower due to preferential evaporation of the nitrate spray before it landed on the heated substrate.

The melt quench technique as described by Akamatsu *et al.* [18] involved mixing carbonates of Sr and Ca with oxides of Bi and Cu to form compositions of 1112, 2212, and 2223. The mixtures were not calcined but coated directly on to single-crystal MgO and melted at 1200 °C. They were cooled to between 700 and 900 °C and held at that temperature for crystallization before cooling further. Film thicknesses were 50–100 μm and the samples were found to have T_0 in the range of 93 K [18].

This study focuses on the phase changes occurring in superconducting thick films printed from a novel paste on single-crystal MgO. A light blue paste was formed by mixing a spray-dried BiSrCaCu nitrate powder with water. Although several authors have suggested using the nitrates for making superconducting powders [19–21] or for spraying directly on to substrates [17], we believe that we are the only group using a nitrate paste to produce superconducting BiSrCaCu oxide films. This method eliminates the repeated calcining and grinding necessary to obtain a single-phase powder, and minimizes compositional differences between the starting solution and the fired film. The nitrate paste is also compatible with screen printing.

The highly reactive paste decomposes during firing to produce the superconducting phases. The relative amounts of the phases are dependent on time, temperature, atmosphere, composition, substrate and dopants. Through control of the time and temperature used to fire the 2212 composition, superconducting thick films with reproducible $T_0 = 85$ K on single-crystal MgO can be obtained.

2. Experimental procedure

Aqueous stock solutions, of 0.1 M bismuth nitrate, strontium nitrate, and copper nitrate, were made. Additional nitric acid was added to the bismuth solution (7.5 ml HNO_3/1 H_2O) in order to dissolve the powder completely and to prevent hydrolysis. A 0.05 M calcium nitrate solution was also prepared. These stock solutions were mixed in equal parts to make the 2212 nitrate solution for spray drying. Additional nitric acid was mixed with this solution to prevent bismuth nitrate from precipitating (20 ml HNO_3/1 H_2O). The spray drying parameters used are listed in Table I. A dry, light blue powder resulted. The powder was characterized by XRD, inductively coupled plasma (ICP), and thermogravimetric analysis (TGA).

When a small amount of water was added to the 2212 nitrate powder (<20 wt %), a light blue paste formed. The 2212 nitrate paste was coated on single-crystal (100) MgO by hand. A slow firing, 3–5 °C min^{-1} to 880° C, was used to decompose the nitrates. Samples were held at 880 °C for 20 min and then furnace cooled. Secondary heat treatments were given by preheating a furnace to a set temperature, inserting the sample for a prescribed time, and then quenching to room temperature. All samples were fired in air. The sintered films were examined by XRD (CuK_α), ICP, and by a scanning electron microscope (SEM) equipped with X-ray microanalysis. The superconducting properties were tested using standard four-point a.c. resistance versus temperature measurements as described by Strom *et al.* [22].

3. Results

The XRD pattern of the starting powder is complex, and $Cu_2(OH)_3NO_3$ and $Sr(NO_3)_2$ were the only phases clearly identified. Carbonates or oxides are not likely to occur due to the lack of carbon groups in the starting solution and due to the low spray-drying temperature (<200 °C). The XRD pattern of the nitrate paste is not significantly different from the dry powder.

TGA results show that the decomposition of the nitrates is complete by 650 °C. The regions of maximum weight loss, indicated by a peak in the derivative curve, have been tentatively assigned to the various phases that decompose based on previous experience with the YBC system [22], the decomposition behaviour of the individual nitrates, and the decomposition temperatures reported in the literature [23]. The Sr and Ca nitrates are the last phases to decompose. Melting and a small amount of evaporation of intermediate reaction products may account for the weight loss at $\gtrsim$ 900 °C.

Chemical analysis by ICP has revealed no changes in stoichiometry within experimental error during firing of the films. As the spray-dried powder is formed at low temperatures, no preferential evaporation of the nitrates occurs. The stoichiometry of the fired film is the same as the starting solution.

The nitrate paste was coated on MgO and given the primary heat treatment. Poorly adhered, black, randomly oriented films were obtained. For short secondary firing times at temperatures less than 890 °C, the

TABLE I Spray-drying parameters – Yamoto model GA-31[a]

Inlet temperature	200 °C
Outlet temperature	80 °C
Aspirator setting	3
Drying air flow	0.23–0.27 $m^3 min^{-1}$
Atomizing pressure	0.29 MPa
Pump rate setting	2

[a] Nozzle-spraying systems air no. 70, liquid no. 2850.

films remained randomly oriented and poorly adhered. Very long secondary heat treatments of 84 h at 875 °C resulted in some grain growth and preferred orientation as indicated by the slightly enhanced intensity of the (0 0 1) lines of the 3.0 nm phase. Some of the 2.4 nm phase was also present in the sample. This film was poorly adhered. At temperatures greater than or equal to 890 °C, however, only short firing times, 10 min or more, were needed to obtain oriented, well-adhered, crack-free films. The thickness of the films decreased to approximately one-half that at 880 °C. The final thicknesses were typically 25–35 μm.

Below 890 °C, the microstructure consisted of randomly oriented, small grains; above 890 °C, however, large, oriented platelets were interspersed with needles (see Figs 1 and 2). X-ray microanalysis revealed that the platelets contained all four elements but some variation in the relative amounts of each was seen within the platelets. The needles contained little, if any, Bi and were extremely high in Ca and Cu compared to the platelets and to the overall composition. Some lightly shaded regions also seen when the samples were examined with the SEM generally appeared to be high in Sr.

In the oriented films fired above 890 °C, both the 3.0 nm phase and the 2.4 nm phase were present. The proportion of each depended on the firing time as shown in Fig. 3 for the 900 °C time series. As the firing time increased, the 2.4 nm phase became dominant. Secondary phases known to be present from the SEM study generally did not show up in XRD due to the high degree of orientation. Occasionally a peak was seen at 30.3° 2θ, but it has not been assigned to a specific phase.

The superconducting transitions of samples treated for increasing amounts of time at 900 °C are shown in Fig. 4. As the time increased, T_0 decreased. Preliminary experiments indicated that some improvement in T_0 could be obtained by preheating the sample at 885 °C before firing at 900 °C as shown in Fig. 5.

The best superconducting transitions, however, were obtained when samples fired at 900 °C were given a secondary heat treatment at 875 °C. The 2.4 nm phase completely disappeared and T_0 values were approximately 85 K as shown in Figs 5c and 6a. This has been found to hold true for several samples.

The 2.4 nm to 3.0 nm phase transition appeared to be reversible as shown in Fig. 7. The 2.4 nm phase

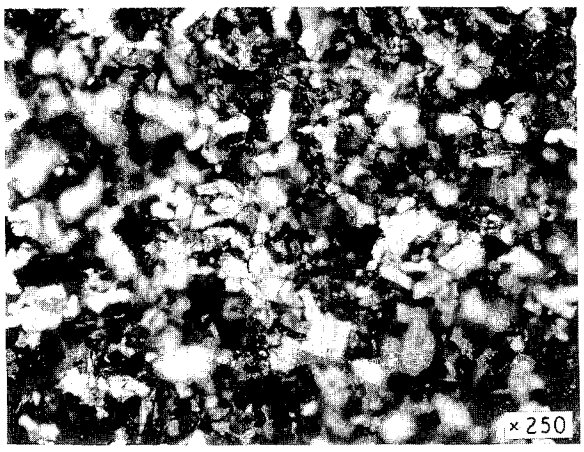

Figure 1 Optical micrograph of randomly oriented grains observed for 2212 thick film samples on single-crystal MgO fired below 890 °C. × 375.

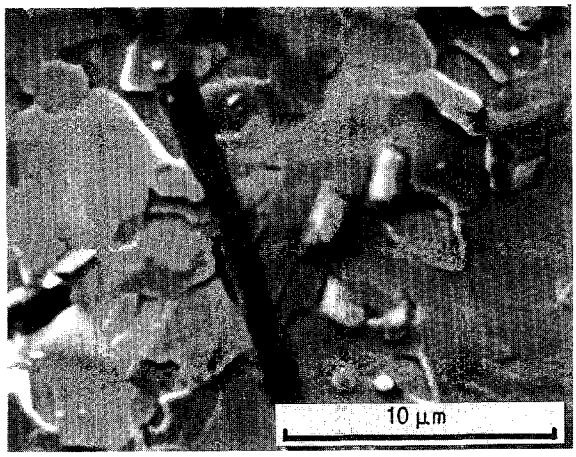

Figure 2 Microstructure of 2212 thick film sample on single-crystal MgO fired at 900 °C for 12 min. Note large oriented platelets, dark coloured needles and lightly coloured, slightly raised regions.

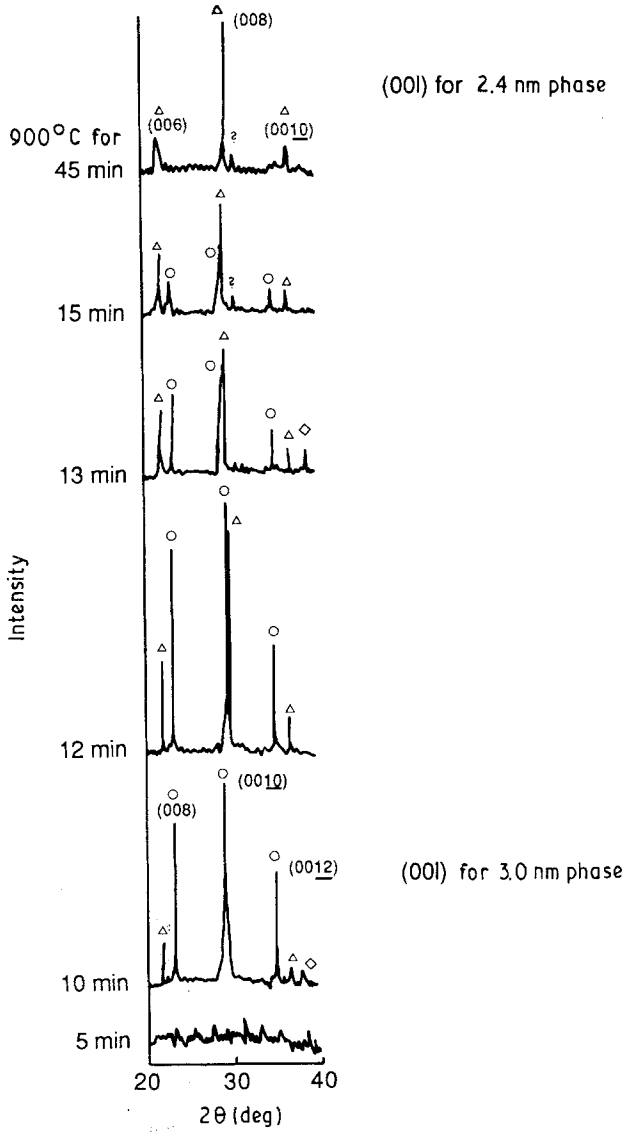

Figure 3 XRD patterns of 2212 thick films on single-crystal MgO fired for various times at 900 °C. Increased firing time correlates to increased amount 2.4 nm phase (△) 2.4 nm phase, (○) 3.0 nm phase; (◇) MgO.

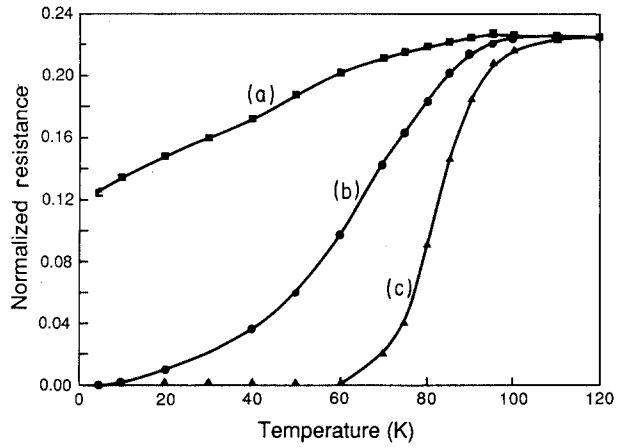

Figure 4 Four-point a.c. R versus T for 2 2 1 2 thick films on single-crystal MgO fired for (a) 15 min, (b) 12 min, (c) 10 min, at 900 °C. R normalized to that of the best film.

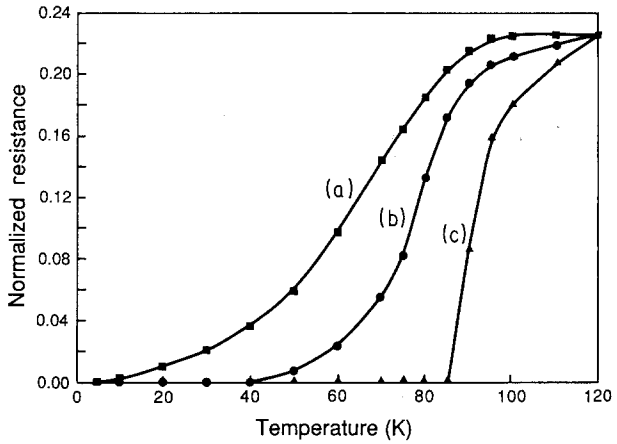

Figure 5 Four-point a.c. R versus T for 2 2 1 2 thick films on single-crystal MgO. (a) 12 min at 900 °C; (b) 2.5 h at 885 °C and 12 min at 900 °C; (c) 4 h at 885 °C, 12 min at 900 °C and 2 h at 875 °C.

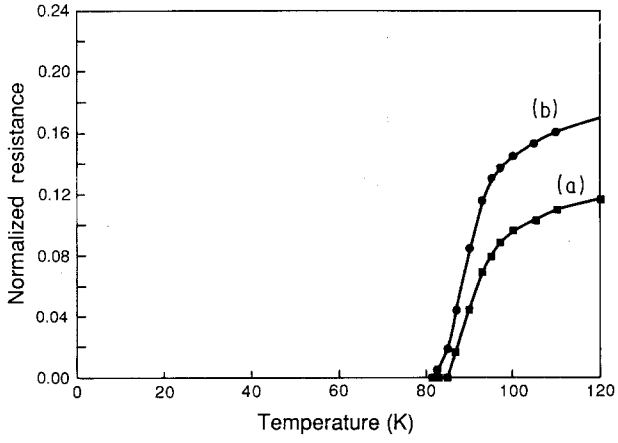

Figure 6 Four-point a.c. R versus T for 2 2 1 2 thick films on single-crystal MgO. (a) Sample fired for 2 h 45 min at 900 °C and 1 h at 875 °C; (b) same sample aged for 2 months at room temperature.

appeared after the 900 °C treatments and converted back to 3.0 nm after the 875 °C treatments. This sample became completely superconducting at 81 K despite the repeated firings.

SEM and X-ray microanalysis of the samples with a post-heat treatment at 875 °C revealed several small, lightly shaded particles distributed across the surface

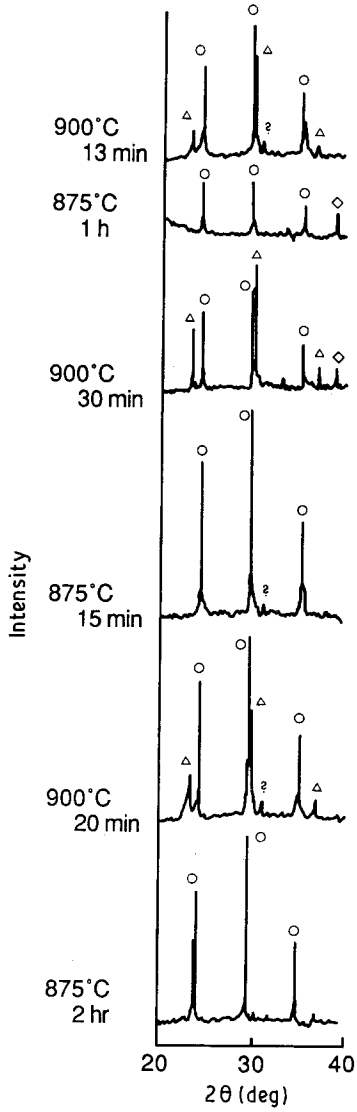

Figure 7 XRD patterns of sample during cycling from 900 °C for 13 min to 875 °C for 2 h. Notice the appearance of the 2.4 nm phase after the 900 °C treatments and disappearance after the 875 °C treatments. (△) 2.4 nm phase, (○) 3.0 nm phase, (◇) MgO.

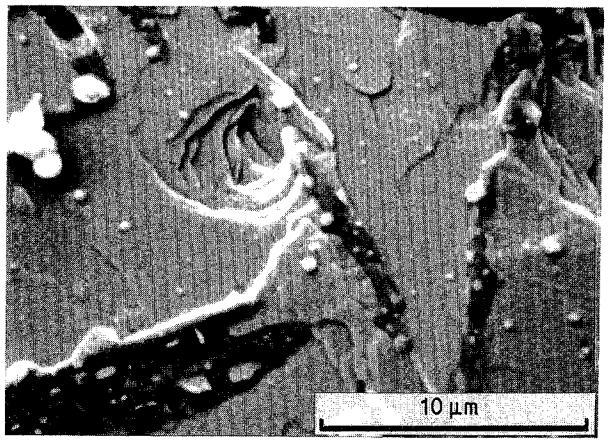

Figure 8 Microstructure of sample fired to 900 °C and given an additional heat treatment at 875 °C as viewed with SEM. Note the large number of lightly coloured particles as compared to the sample in Fig. 2.

(see Fig. 8). These particles were found to be rich in Sr. Under the optical microscope, the platelets, which were very smooth and uniform after the 900 °C treatment, began to show small dark spots after the 875 °C

treatment. The dark spots appeared to correlate to the lightly shaded particles seen by SEM analysis (cf. Fig. 9a and b). The number and size of the dark spots increased with the age of the sample as shown in Fig. 9c. This is true for samples processed under a variety of conditions. The sample in Fig. 9b was aged at room temperature for 2 months (Fig. 9c) and tested again for superconductivity. Some degradation was seen as shown in Fig. 6b by the higher resistance and lower T_0.

4. Discussion

Thick films with a reproducible T_0 of 85 K have been achieved on single-crystal MgO through control of the relative amounts of the 2.4 and 3.0 nm phases. In Fig. 3 it was shown that the amount of the 2.4 nm phase increased with increasing time at 900 °C. T_0 values for these samples decreased as the proportion of the 2.4 nm phase increased, as shown in Fig. 4. T_c remained fairly constant for these samples. The overall result was an increase in the transition width. The pretreatment at 875 °C before firing at 900 °C resulted in both a decrease in the amount of the 2.4 nm phase and an increase in T_0. Heat treatment at 875 °C after firing at 900 °C gave the highest T_0 value and narrowest transitions. The 2.4 nm phase was not detected in these samples. These observations indicate that if the 3.0 nm phase is present, the transition starts above 85 K. The final width of the transition curve may result from both the amount and spatial distribution of the 2.4 nm phase relative to the 3.0 nm phase.

It has been clearly shown by several research groups that the superconducting 2.4, 3.0 and 3.7 nm phases form platelets [24–26]. The 3.0 nm and 3.7 nm phases have been found to segregate both within grains (intergrowths) [9, 25], and on a large multigrain scale [26]. If the 2.4 and 3.0 nm phases segregate in a similar manner, the intergrowths would explain the platelet-to-platelet composition variation observed here by X-ray microanalysis. Some large-scale variation in colour was seen for a few samples as described by Yoshitake *et al.* [26], but we were unable to correlate this to a variation in stoichiometry through X-ray dot mapping.

Large needles deficient in Bi have been observed by several researchers. The needles we have observed appear closest to those described by Hazen *et al.* [24]. They are most likely a solid solution of Sr in Ca_2CuO_3. Togano *et al.* [13] observed several white particles and interpreted them to be another SrCaCu oxide compound. Some of the lightly shaded particles we have observed also appear to have bismuth. Further work is being done to identify more clearly the secondary phases because they may be important in determining the intermediate reaction path for the 2.4 nm to 3.0 nm phase transition.

Kanai *et al.* [6] suggest that the 2.4 nm phase crystallizes initially but transforms to the 3.0 nm phase above 700 °C. At 840 °C and above, they suggest that the 3.0 nm phase decomposes back to the 2.4 nm and 3.7 nm phases as shown in the following reaction

$$\underset{3.0\text{ nm}}{Bi_4(Ca, Sr)_6Cu_4O_x} \rightarrow \underset{2.4\text{ nm}}{Bi_2(Ca, Sr)_2CuO_x} + \underset{3.7\text{ nm}}{Bi_2(Ca, Sr)_4Ca_3O_x} \quad (1)$$

They further state that the 37 nm phase may decompose further into nonsuperconducting phases because it is not stable above 840 °C. Kanai *et al.* [6] do not mention any needles and their potential relationship to the 3.0 nm to 2.4 nm phase change. Also, they do

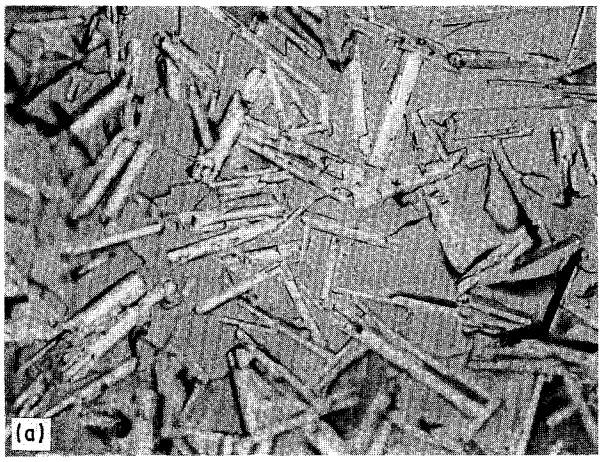

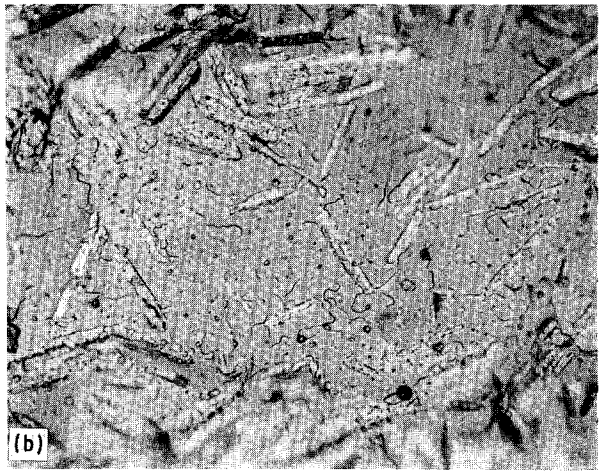

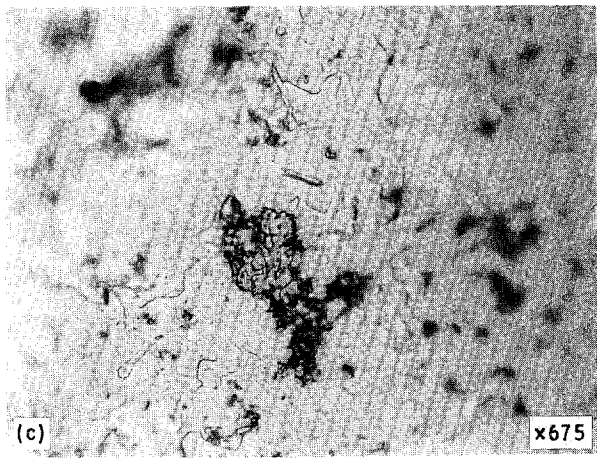

Figure 9 Microstructure as viewed through the optical microscope. (a) Large smooth platelets and needles after 900 °C treatment; (b) black spots appear after 875 °C treatment; (c) black spots increase in size after ageing for 2 months. × 750

not discuss the reverse transformation from 2.4 nm to 3.0 nm.

The temperature at which Kanai *et al.* [6] believe the 3.0 nm to 2.4 nm phase transition occurs is 50 °C lower than that we have found. Their results for firing in air are closer to those which we found for firing in argon. We suggest that by quenching their samples from 1050 °C to 77 K, they have created a large number of oxygen vacancies. The Cu_2O phase they observed supports this theory. When we fire in argon similar vacancies may be created, causing a lowering in the melting point and thereby the sintering temperature as reported by several groups [27–31]. According to Inoue *et al.* [27], the melting point for the 1 1 1 2 composition is 840 °C in N_2, 880 °C in air, and 910 °C in O_2.

It has been suggested that the 3.0 nm phase can be transformed to the 2.4 nm phase by the deletion of a CuO_2 and a Ca/Sr layer, or vice versa [5, 6]. This may explain why the appearance of the 2.4 nm phase at 890 °C and above is accompanied by Ca, Sr, Cu-rich needles. We see no need for the 3.7 nm phase as an intermediate in this reaction. We have neither detected the 3.7 nm phase by XRD nor seen decreases in the resistance at 110 K to indicate it is present. It is important to note that we worked with the 2 2 1 2 composition and Kanai *et al.* [6] worked with the 1 1 1 2 composition, however.

The transformation we have observed of the 2.4 nm phase back to 3.0 nm at 875 °C could be due to a reaction between the needles and the 2.4 nm phase. The needles, however, were still present after 2 h at 875 °C. The model we propose is for two of the 2.4 nm phase unit cells to transform to a 3.0 nm cell by losing two bismuth oxide layers and one strontium oxide layer as shown in Fig. 10. Sr, Bi-rich particles were found after the 875 °C treatment.

If the 3.0 nm phase decomposes to give the 2.4 nm phase plus needles at 900 °C and two units of the 2.4 nm phase decompose to give the 3.0 nm phase plus Sr, Bi-rich particles at 875 °C, this reaction should not be fully reversible. The amount of the superconducting phase should steadily decrease as the number of needles and white particles increases. This may explain the lower T_0 for the cycled sample (Fig. 7). Clearly one would like to minimize not only the amount of the 2.4 nm phase but also the amount of the nonsuperconducting phases (needles and white particles). One would still like to obtain the orientation and good adherence to the substrate which is possible above 890 °C, however.

Good adherence and orientation appear to be the result of firing near the melting point. The high–low firing used by several groups to enhance the 110 K phase formation in the 1 1 1 2 composition takes advantage of a temperature near the melting point to sinter their films [2, 14, 15, 32]. The enhancement of the 3.7 nm phase over the 3.0 nm phase may be similar to the enhancement of the 3.0 nm phase over the 2.4 nm phase we have observed. Hoshino *et al.* [15] and Nakamori *et al.* [14] observed similar orientation to what we have found, in their thick films fired near the melting point. Nakamori *et al.* [14] show a film fired first at 890 °C and then at 870 °C. The micrograph shows both needles and lightly shaded particles similar to those found in our films, but the authors do not discuss them.

The ageing effect seen in our films may be similar to that reported for YBC. $SrCO_3$ and $CaCO_3$ have a high free energy of formation similar to $BaCO_3$ [33].

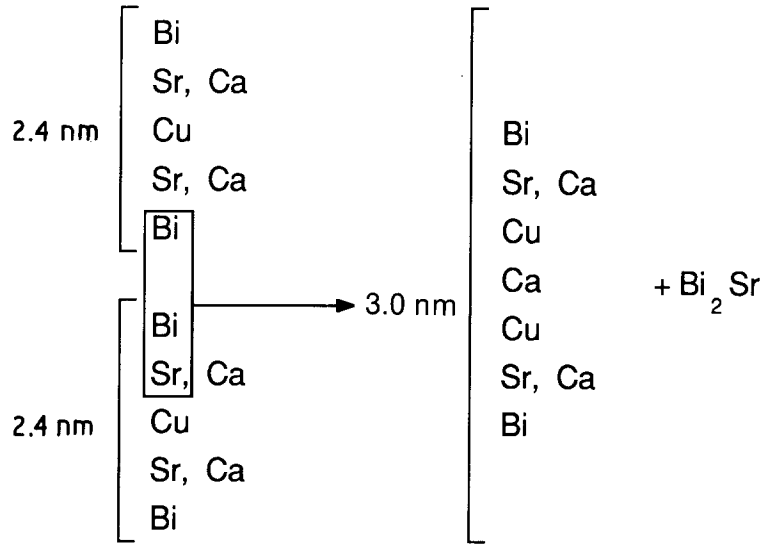

$$2(Bi_2(Sr_{1.5}Ca_{0.5})Cu_1O_x) \longrightarrow Bi_4Sr_3Ca_1Cu_2O_x \longrightarrow Bi_2Sr_2Ca_1Cu_2O_x + Bi_2SrO_x$$

$$2(2.4\,nm) \longrightarrow 3.0\,nm + Bi_2SrO_x$$

Figure 10 Proposed model for phase transformation from 2.4 nm to 3.0 nm phase. Two 2.4 nm unit cells transform to one 3.0 nm unit cell by losing two bismuth oxide layers and one strontium oxide layer. Sr is preferentially lost because Ca is favoured between the two Cu layers due to its smaller size. The displaced Bi and Sr coalesce into Sr, Bi-rich particles.

It has been reported that because the reaction to form $BaCO_3$ is so favourable, it may form at room temperature by the BaO layer in YBC reacting with H_2O and CO_2 in the atmosphere [34, 35]. Formation of $SrCO_3$ and/or $CaCO_3$ may also be very favourable, particularly in films where Sr- and Ca-rich phases have segregated. XRD did not detect any $SrCO_3$ or $CaCO_3$ present on the surface of the aged films. Individual crystallites of the carbonates may be too small to detect by XRD, however. Further work needs to be done to ascertain whether the particles formed on the surface of the aged film are indeed $SrCO_3$ or $CaCO_3$. The degradation in T_0 for aged films could result from the leaching of Sr and/or Ca from the 3.0 nm phase.

5. Conclusion

A novel method for producing superconducting thick films of 2212 on single-crystal MgO has been presented. A reproducible T_0 of 85 K was achieved by controlling ratio of the 2.4 nm to 3.0 nm phases. Possible reaction paths for the 3.0 nm to 2.4 nm and 2.4 nm to 3.0 nm phase transformations have been discussed. Further work needs to be done to minimize the nonsuperconducting phases including any $SrCO_3$ or $CaCO_3$ which may be forming as a result of ageing in an environment containing CO_2 and H_2O.

Acknowledgements

We thank Jose Mir and Dilip Chatterjee for valuable discussions, Arun Mehrotra for his input on argon heat treatments, Ralph Nicholas for DTA/TGA measurements, Edward McLean for chemical analysis by ICP, and Craig Barnes and David Duval for XRD.

References

1. J. AKIMITSU, A. YAMAZAKI, H. SAWA and H. FUJIKI, *Jpn J. Appl. Phys.* **26** (1987) L2080.
2. H. MAEDA, Y. TANAKA, M. FUKUTOMI and T. ASANO, *ibid.* **27** (1988) L209.
3. E. TAKAYAMA-MUROMACHI, Y. UCHIDA, A. ONO, F. IZUMI, M. ONODA, Y. MATSUI, K. KOSUDA, S. TAKEKAWA and K. KATO, *ibid.* **27** (1988) L365.
4. M. OHKUBO, *ibid.* **27** (1988) L1271.
5. E. TAKAYAMA-MUROMACHI, Y. UCHIDA, Y. MATSUI, M. ONODA and K. KATO, *ibid.* **27** (1988) L556.
6. T. KANAI, T. KUMAGAI, A. SOETA, T. SUZUKI, K. AIHARA, T. KAMO and S. MATSUDA, *ibid.* **27** (1988) L1435.
7. M. ONODA, A. YAMAMOTO, E. TAKAYAMA-MUROMACHI and S. TAKEKAWA, *ibid.* **27** (1988) L833.
8. Y. SYONO, K. HIRAGA, N. KOBAYASHI, M. KIKUCHI, K. KUSABA, T. KAJITANI, D. SHINDO, S. HOSOYA, A. TOKIWA, S. TERADA and Y. MUTO, *ibid.* **27** (1988) L569.
9. R. RAMESH, G. THOMAS, S. M. GREEN, YU MEI, C. JIANG and H. L. LUO, *Appl. Phys. Lett.* **53** (1988) 1759.
10. P. L. GAI and P. DAY, *Physica C* **152** (1988) 335.
11. A. MAEDA, T. YABE, H. IKUTA, Y. NAKAYAMA, T. WADA, S. OKUDA, T. ITOH, M. IZUMI, K. UCHINOKURA, S. UCHIDA and S. TANAKA, *Jpn J. Appl. Phys.* **27** (1988) L661.
12. T. WADA, N. SUZUKI, A. MAEDA, S. UCHIDA, K. UCHINOKURA and S. TANAKA, *ibid.* **27** (1988) L1031.
13. K. TOGANO, H. KUMAKURA, H. MAEDA, E. YANAGISAWA and K. TAKAHASHI, *Appl. Phys. Lett.* **53** (1988) 1329.
14. T. NAKAMORI, H. ABE, T. TAKAHASHI, T. KANAMORI and S. SHIBATA, *Jpn J. Appl. Phys.* **27** (1988) L649.
15. K. HOSHINO, H. TAKAHARA and M. FUKUTOMI, *ibid.* **27** (1988) L1297.
16. T. HASHIMOTO, T. KOSAKA, Y. YOSHIDA, K. FUEKI and H. KOINUMA, *ibid.* **27** (1988) L384.
17. H. NOBUMASA, K. SHIMIZU, Y. KITANO and T. KAWAI, *ibid.* **27** (1988) L1669.
18. Y. AKAMATSU, M. TATSUMISAGO, N. TOHGE, S. TSUBOI and T. MINAMI, *ibid.* **27** (1988) L1696.
19. E. C. BEHRMAN *et al.*, *Adv. Ceram. Mater.* **2** (1987) 539, special issue.
20. M. L. KAPLAN and J. J. HAUSER, *Mater. Res. Bull.* **23** (1988) 287.
21. S. DAVISON, K. SMITH, Y.-E. ZHANG, J.-H. LIU, R. KERSHAW, K. DWIGHT, P. H. KIEGER and A. WOLD, in "Chemistry of High Temperature Superconductors," edited by D. L. Nelson, M. S. Whittingham and T. F. George (American Chemical Society, Washington, DC, 1987) pp. 65–78.
22. L. STROM, E. CARNALL, S. FERRANTI and J. MIR, *J. Mater. Sci.*
23. R. W. WEAST (ed.) "CRC Handbook of Chemistry and Physics" (CRC Press, West Palm Beach, Florida, 1978).
24. R. HAZEN, C. T. PREWITT, R. J. ANGEL, N. L. ROSS, L. W. FINGER, C. G. HADIDIACOS, D. R. VEBLEN, P. J. HEANEY, P. H. HOR, R. L. MENG, Y. Y. SUN, Y. Q. WANG, Y. Y. XUE, Z. J. HUANG, L. GAO, J. BECHTOLD and C. W. CHU, *Phys. Rev. Lett.* **60** (1988) 1174.
25. S. IKEDA, H. ICHINOSE, T. KIMURA, T. MATSUMOTO, H. MAEDA, Y. ISHIDA and K. OGAWA, *Jpn J. Appl. Phys.* **27** (1988) L999.
26. T. YOSHITAKE, T. SATOH, Y. KUBO and H. IGARASHI, *ibid.* **27** (1988) L1089.
27. O. INOUE, S. ADACHI and S. KAWASHIMA, *ibid.* **27** (1988) L347.
28. Y. OKA, N. YAMAMOTO, A. YUBA, H. KIAGUCHI and J. TAKADA, *ibid.* **27** (1988) L1429.
29. U. ENDO, S. KOYAMA and T. KAWAI, *ibid.* **27** (1988) L1476.
30. H. TERADA, T. IDO and S. MUTO, *ibid.* **27** (1988) L1219.
31. I. IGUCHI and A. SUGISHITA, *Physica C* **152** (1988) 228.
32. Y. TANAKA, M. FUKUTOMI, T. ASANO and H. MAEDA, *Jpn J. Appl. Phys.* **27** (1988) L548.
33. W. M. LATIMER, "The Oxidation States of the Elements and Their Potentials in Aqueous Solutions" (Prentice-Hall, New York, 1952).
34. J. WANG, R. STEVENS and J. BULTITUDE, *J. Mater. Sci.* **23** (1988) 3393.
35. D. MAJUMDAR, D. CHATTERJEE and G. PAZ-PUJALT, *Physica C* **158** (1989) 413.

Received 18 September 1989
and accepted 9 April 1990